Letters

Influence of PLL on Stability of Interconnected Grid-Forming and Grid-Following Converters

Yang Wu, *Member, IEEE*, Heng Wu, *Senior Member, IEEE*, Fangzhou Zhao, *Member, IEEE*, Zejie Li, *Student Member, IEEE*, and Xiongfei Wang, *Fellow, IEEE*

***Abstract*—This letter analyzes the impact of a phase-locked loop (PLL) on small-signal stability in a system of interconnected grid-forming and grid-following (GFL) converters. It identifies an undiscovered instability phenomenon, i.e., the system is prone to unstable when the bandwidth of PLL used with GFL converter is low. Experiments validate the theoretical analysis.**

***Index Terms*—Grid-following (GFL) converter, grid-forming (GFM) converter, phase-locked loop (PLL), small-signal stability.**

I. Introduction

VOLTAGE-SOURCE converters (VSCs) are widely found in power grids. VSCs can be controlled in grid-following (GFL) or grid-forming (GFM) modes. The GFM-VSC is operated as voltage source behind an impedance, which forms the grid voltage [1], [2]. The GFL-VSC is then synchronized to the grid, commonly by using a phase-locked loop (PLL) [3]. Interconnected GFM- and GFL-VSC systems are increasingly deployed in modern power grids, e.g., the high-voltage dc-connected wind power plants [4].

The dynamic impact of PLL on the stability of GFL-VSCs is extensively reported in the recent literature. It is revealed that the PLL introduces a negative damping within its control bandwidth [5], which can manifest instability when GFL-VSC is connected to a weak grid with high grid impedance [6]. Yet, most work is on the GFL-VSC connected to the weak grid that has a low short-circuit ratio [7], [8]. The influence of PLL on the stability of interconnected GFM- and GFL-VSC systems is not fully revealed. The work [4] identifies a maximum PLL bandwidth for stable operation of interconnected GFM- and GFL-VSC systems. However, as will be demonstrated in this letter, a low bandwidth of the PLL can also destabilize the system, which differs from the GFL-VSC connected to a high-impedance grid. This unique phenomenon is induced by the interaction between synchronization controllers of converters [the power synchronization (PSC) controller of GFM-VSC and the PLL of GFL-VSC], which has rarely been reported.

The rest of this letter is organized as follows. Section II presents the small-signal modeling of interconnected GFM- and GFL-VSC systems, which explicitly characterize the parametric impact of PLL. Section III demonstrates system instability with different PLL bandwidths, which is followed by the experimental validation in Section IV. Finally, Section V concludes this letter.

Manuscript received 23 April 2024; revised 28 May 2024 and 27 June 2024; accepted 28 June 2024. Date of publication 2 July 2024; date of current version 4 September 2024. This work was supported by the European Union's Horizon 2020 Research and Innovation Programme through the Marie Skłodowska-Curie under Grant 101107634 (PhyDAWN). *(Corresponding author: Xiongfei Wang.)*

Yang Wu, Heng Wu, Fangzhou Zhao, and Zejie Li are with the Department of Energy, Aalborg University, 9220 Aalborg, Denmark (e-mail: yawu@energy.aau.dk; hew@energy.aau.dk; fzha@energy.aau.dk; zl@energy.aau.dk).

Xiongfei Wang is with the Division of Electric Power and Energy Systems, KTH Royal Institute of Technology, 10044 Stockholm, Sweden, and also with the Department of Energy, Aalborg University, 9220 Aalborg, Denmark (e-mail: xiongfei@kth.se).

Color versions of one or more figures in this article are available at https://doi.org/10.1109/TPEL.2024.3421960.

Digital Object Identifier 10.1109/TPEL.2024.3421960

II. System Description and Modeling

A. System Description

The studied system of interconnected GFM- and GFL-VSC is shown in Fig. 1(a). Both the converters are filtered by L filters, which are represented by L_{GFM} and L_{GFL}, respectively. The transmission line connecting the two converters is represented by an inductor L_{Line}. The grid voltage is regulated by the GFM-VSC with PSC controller, and the GFL-VSC tracks the phase angle of the grid by PLL. Cascaded power controller and current controller in PI form are also applied to regulate the GFL-VSC. v_{GFL} and i_{GFL} represent the voltage and current measured for the control of the GFL-VSC, while v_{GFM} and i_{GFM} are similarly defined for the GFM-VSC. The dc links of both converters are assumed to be stiff, with $V_{L\mathrm{dc}}$ and $V_{M\mathrm{dc}}$ modeled as constant dc voltage sources. This is because the voltage of dc link can be controlled by back-to-back converters or energy storage systems [9], [10]. Therefore, the dc-link dynamics have been neglected in the modeling for simplicity.

In this letter, the GFM converter is considered as the power absorbing end, while the GFL converter is considered as the power outputting end. This studied structure serves as a representative for future power-electronic-based power systems [1], [11], [12], [13]. A practical case comes from the PROMOTioN Project by the European Union [14], as shown in Fig. 1(b). A reported system design in this project includes an offshore

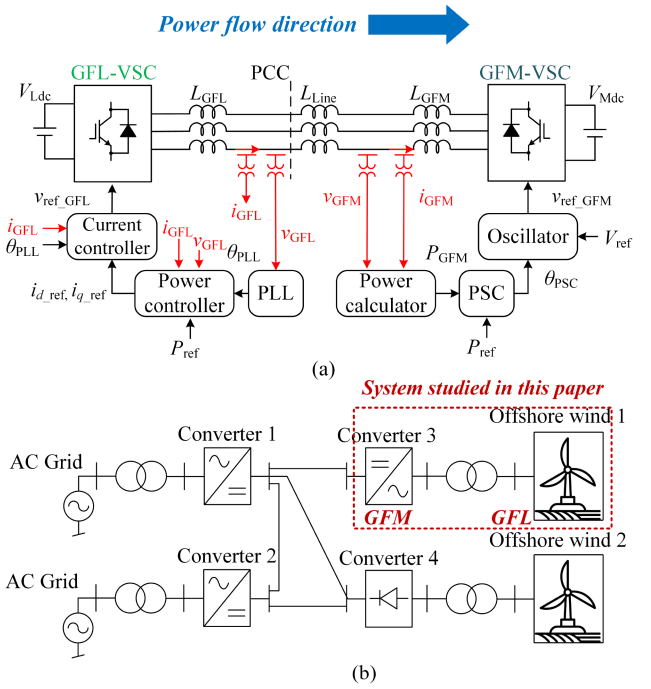

Fig. 1. (a) Schematic diagram of the studied interconnected GFM- and GFL-VSC. (b) Practical case of the studied system from [14].

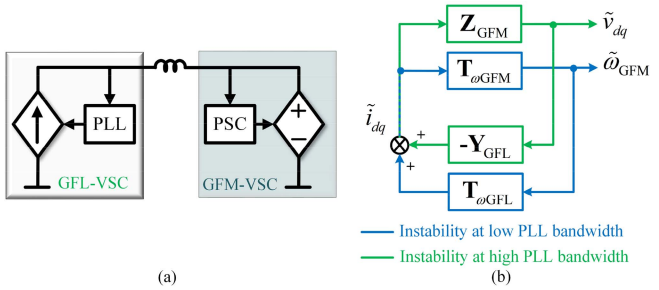

Fig. 2. (a) Equivalent circuit representation of the interconnected GFM- and GFL-VSC system and (b) small-signal model for the studied system. A minus sign exists in -$\mathbf{Y}_{\mathrm{GFL}}$ as reference current direction is defined as flowing out from the GFL-VSC.

windfarm connected to a modular multilevel converter (MMC) station via HVac interconnection. Normally, the power converters in windfarms use GFL control for referenced power output. Therefore, the MMC needs to use the GFM control to regulate the local voltage and phase angle for the GFL-converters in the wind farms to track.

B. Physical Insights on Instability Under Low PLL Bandwidth

Fig. 2(a) illustrates the equivalent circuit representation of the studied system with synchronization controllers (i.e., PLL and PSC) highlighted. Different from the GFL-VSC connected to weak grid where the grid frequency is fixed, the grid frequency of the studied system is regulated by PSC of GFM-VSC and has its own dynamics. By using low PLL bandwidth, the GFL-VSC may lose track of such grid frequency dynamics, thereby inducing adverse dynamics on its output current. Such output

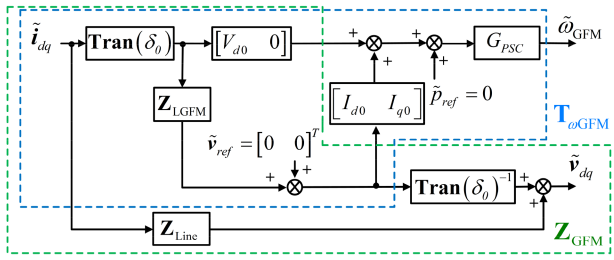

Fig. 3. Block diagram for the small-signal model of GFM-VSC.

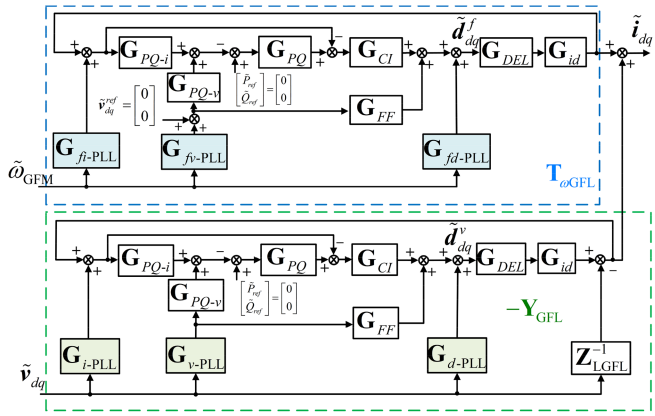

Fig. 4. Block diagram for the small-signal model of GFL-VSC.

current of GFL-VSC with adverse dynamics will flow into the GFM-VSC, and further exacerbate system frequency dynamics via PSC. This chain of reaction, as will be rigorously demonstrated later in this work, actually forms a positive feedback loop and would destabilize the system.

C. Small-Signal Modeling of the System

To characterize the parametric impact of PLL on system stability, a small-signal modeling methodology proposed in [2] is used in this letter. The fundamental frequency dynamics generated by the GFM-VSC is treated as an additional terminal of the impedance model. Meanwhile, the entire system is modeled in the reference frame associated with this dynamic fundamental frequency.

The small-signal model of the interconnected converters is shown in Fig. 2(b). $\tilde{v}_{dq}$ and $\tilde{i}_{dq}$ represent the voltage and current perturbations at the point of common coupling (PCC) point, which are expressed in the *dq*-frame rotating with dynamic fundamental frequency. $\tilde{\omega}_{\mathrm{GFM}}$ represents the fundamental frequency dynamics generated by the GFM-VSC, which is in angular format for simplicity. $\mathbf{Z}_{\mathrm{GFM}}$ represents the terminal impedance of the GFM-VSC, and $\mathbf{Y}_{\mathrm{GFL}}$ represents the terminal admittance of the GFL-VSC. $\mathbf{T}_{\omega\mathrm{GFM}}$ describes the response of fundamental frequency under the input current perturbations of the GFM-VSC, while $\mathbf{T}_{\omega\mathrm{GFL}}$ describes the response of output current under fundamental frequency perturbations of the GFL-VSC.

Furthermore, the block diagrams for the small-signal model of GFM- and GFL-VSC can be obtained as Figs. 3 and 4, following the modeling methods in [2] and [15], respectively.

For the GFM-VSC, $\mathbf{Z}_{\mathrm{GFM}}$ and $\mathbf{T}_{\omega\mathrm{GFM}}$ can be expressed as

$$\mathbf{Z}_{\mathrm{GFM}} = \mathbf{Z}_{\mathrm{Line}} + \mathbf{Tran}(\delta_0)^{-1}\mathbf{Z}_{\mathrm{LGFM}}\mathbf{Tran}(\delta_0) \quad (1)$$

$$\mathbf{T}_{\omega\mathrm{GFM}} = G_{PSC}\left([I_{d0}, I_{q0}]\,\mathbf{Z}_{\mathrm{LGFM}}\mathbf{Tran}(\delta_0) + [V_{d0}, 0]\,\mathbf{Tran}(\delta_0)\right) \quad (2)$$

where $\mathbf{Z}_{\mathrm{LGFM}}$ and $\mathbf{Z}_{\mathrm{Line}}$ represent the impedance matrices of L_{GFM} and L_{Line}. Take $\mathbf{Z}_{\mathrm{LGFM}}$ as an example:

$$\mathbf{Z}_{\mathrm{LGFM}} = \begin{bmatrix} sL_{\mathrm{GFM}} & -\omega_{\mathrm{GFM0}}L_{\mathrm{GFM}} \\ \omega_{\mathrm{GFM0}}L_{\mathrm{GFM}} & sL_{\mathrm{GFM}} \end{bmatrix} \quad (3)$$

where ω_{GFM0} represents the steady-state operating frequency of GFM-VSC. $\mathbf{Tran}(\delta_0)$ is introduced by the phase angle difference across the line inductance L_{Line}. V_{d0}, I_{d0}, and I_{q0} represent the steady-state voltage aligned to d-axis, and currents in dq-axes. G_{PSC} denotes the transfer function of PSC:

$$G_{\mathrm{PSC}} = (G_p\omega_f)/(s+\omega_f). \quad (4)$$

where G_p is the droop parameter and ω_f is the cutoff frequency of the low-pass filter.

For the GFL-VSC, the block diagrams of $\mathbf{T}_{\omega\mathrm{GFL}}$ and $\mathbf{Y}_{\mathrm{GFL}}$ comprise many identical transfer function matrices, including power calculation matrices $\mathbf{G}_{PQ\text{-}i}$ and $\mathbf{G}_{PQ\text{-}v}$, power control $\mathbf{G}_{PQ}$, current control $\mathbf{G}_{CI}$, feedforward control $\mathbf{G}_{FF}$, delay $\mathbf{G}_{DEL}$, and duty ratio to current matrix $\mathbf{G}_{id}$. Detailed expressions for $\mathbf{Y}_{\mathrm{GFL}}$ and $\mathbf{T}_{\omega\mathrm{GFL}}$ can be found in [5] and [15], whose main difference lies in the influence of PLL on the controller current, voltage and duty ratio. Such influence is reflected by $\mathbf{G}_{fi\text{-PLL}}$, $\mathbf{G}_{fv\text{-PLL}}$, and $\mathbf{G}_{fd\text{-PLL}}$ in $\mathbf{T}_{\omega\mathrm{GFL}}$, while by $\mathbf{G}_{i\text{-PLL}}$, $\mathbf{G}_{v\text{-PLL}}$, and $\mathbf{G}_{d\text{-PLL}}$ in $\mathbf{Y}_{\mathrm{GFL}}$. This difference roots in the responses of PLL phase angle from the frequency or voltage perturbations. For example, the influence on controller current by the PLL differs as follows:

$$\mathbf{G}_{fi-\mathrm{PLL}} = \begin{bmatrix} 0 & I_{q0}G_{f\mathrm{PLL}} \\ 0 & -I_{d0}G_{f\mathrm{PLL}} \end{bmatrix}, \mathbf{G}_{i-\mathrm{PLL}} = \begin{bmatrix} 0 & I_{q0}G_{\mathrm{PLL}} \\ 0 & -I_{d0}G_{\mathrm{PLL}} \end{bmatrix}. \quad (5)$$

The transfer function $G_{f\mathrm{PLL}}$, which describes the response of PLL angle to frequency perturbations, can be expressed as [15]

$$G_{f\mathrm{PLL}} = -\frac{1}{s + (k_{p\mathrm{PLL}} + k_{i\mathrm{PLL}}/s)\,V_{d0}} \quad (6)$$

where $k_{p\mathrm{PLL}}$ and $k_{i\mathrm{PLL}}$ represent the proportional and integral gain of the PLL. By contrast, in traditional $\mathbf{Y}_{\mathrm{GFL}}$ modeling, the response of PLL phase angle to voltage perturbations is [5]

$$G_{\mathrm{PLL}} = \frac{(k_{p\mathrm{PLL}} + k_{i\mathrm{PLL}}/s)}{s + (k_{p\mathrm{PLL}} + k_{i\mathrm{PLL}}/s)\,V_{d0}}. \quad (7)$$

Hence, the impact of PLL on stability may exhibit unique characteristics within the studied system, which is associated with the system frequency dynamics.

To characterize this unique impact of PLL under frequency perturbations, assume a positive frequency disturbance $\tilde{\omega}_{\mathrm{GFM}}$ occurs and the PCC voltage rotates from v_d to v'_d. The PLL will then try to maintain synchronization with the PCC voltage by rotating the current vector from i_d to i'_d, leading to a positive $\tilde{i}_q$. The vector illustration is shown in Fig. 5. The perturbation on d-axis current is neglected due to a small value.

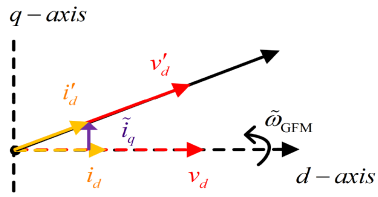

Fig. 5. Vector diagram characterization of $T_{\omega\mathrm{GFL}}$. (The reference current direction is defined as flowing out from the GFL-VSC.)

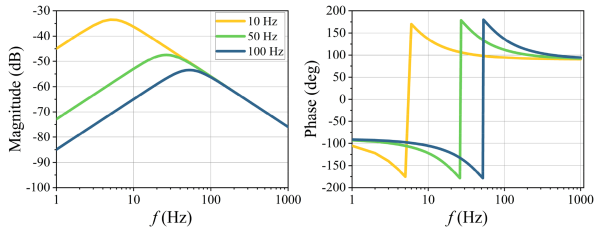

Fig. 6. Bode plot of $G_{f\mathrm{PLL}}$ under different PLL bandwidths.

This positive $\tilde{i}_q$ will further induce positive frequency disturbance through (2), helping to exacerbate the original disturbance on frequency by forming a positive feedback. Furthermore, (6) has shown that low PLL bandwidth will amplify the current response ($\mathbf{T}_{\omega\mathrm{GFL}}$) under frequency disturbances due to the enlarged amplitude of $G_{f\mathrm{PLL}}$, as shown in Fig. 6. Therefore, a low PLL bandwidth will enlarge this positive feedback, eventually resulting in system instability.

The instability phenomenon analyzed above will not be influenced by the power flow direction. This is because the instability is related to the exacerbation of frequency dynamics through the interaction of PLL and PSC, which will still exist under an opposite power flow direction. Moreover, as this kind of instability is induced by the positive feedback loop for system frequency dynamics, it will still exist with a load between the two converters, as long as the proportion between the load and GFL-VSC capacity is within a certain range. The aforementioned modeling and analysis for system instability can still be applied, only with part of the output current from the GFL-VSC drawn by the connected load.

III. Stability Analysis for Different PLL Bandwidth

To further explore the influence of PLL bandwidth on system stability, stability assessment will be conducted with return ratio matrix $\mathbf{L}$ formulated as

$$\mathbf{L} = \mathbf{Y}_{\mathrm{GFL}}\mathbf{Z}_{\mathrm{GFM}} - \mathbf{T}_{\omega\mathrm{GFL}}\mathbf{T}_{\omega\mathrm{GFM}}. \quad (8)$$

According to the generalized Nyquist stability criterion [16], the system will be stable if and only if the eigenloci of $\mathbf{L}$ do not encircle the (-1+j0) point in the complex plane.

A. Stability Analysis With High PLL Bandwidth

By using high PLL bandwidth, the interaction between synchronization controllers $\mathbf{T}_{\omega\mathrm{GFL}}\mathbf{T}_{\omega\mathrm{GFM}}$ can be approximated as zero, due to an attenuated amplitude of $\mathbf{T}_{\omega\mathrm{GFL}}$, as analyzed in Section II-C. Therefore, $\mathbf{L} \approx \mathbf{Y}_{\mathrm{GFL}}\mathbf{Z}_{\mathrm{GFM}}$. According to (1), $\mathbf{Z}_{\mathrm{GFM}}$ is determined by the line inductance L_{Line} and the

converter filter inductance L_{GFM}. As the value of L_{GFM} is normally within 0.1 per unit (p.u.) (and usually smaller than the line impedance L_{Line}) [17], $\mathbf{Z}_{\mathrm{GFM}}$ can be approximated as $\mathbf{Z}_{\mathrm{Line}}$. Hence, system instability at high PLL bandwidth will be similar to that in conventional GFL-VSC operation connected to a weak grid [5]. Instability will appear due to the negative incremental conductance characteristic in the qq-channel of $\mathbf{Y}_{\mathrm{GFL}}$ within the PLL bandwidth. Furthermore, the increase of PLL bandwidth may have a negative influence on system stability due to the widened frequency range of this negative damping.

B. Stability Analysis With Low PLL Bandwidth

With low PLL bandwidth, the instability now appears due to the interaction between synchronization controllers. By analyzing (2) and (6), such interaction happens at low frequencies due to the attenuated amplitudes of both $\mathbf{T}_{\omega\mathrm{GFL}}$ and $\mathbf{T}_{\omega\mathrm{GFM}}$ at high frequencies. Hence, some approximations can be made to simplify the analysis: 1) s is approximated as 0 for the calculation of $\mathbf{Z}_{\mathrm{GFM}}$ and $\mathbf{T}_{\omega\mathrm{GFM}}$; 2) the GFL-VSC is considered to operate at unity power factor, and only the dominant diagonal elements $Y_{\mathrm{GFL}\,dd}$ and $Y_{\mathrm{GFL}\,qq}$ in $\mathbf{Y}_{\mathrm{GFL}}$ are considered [5]. Therefore, $\mathbf{Y}_{\mathrm{GFL}}\mathbf{Z}_{\mathrm{GFM}}$ now becomes

$$\begin{aligned}&\mathbf{Y}_{\mathrm{GFL}}\mathbf{Z}_{\mathrm{GFM}}\\&\approx\begin{bmatrix}Y_{\mathrm{GFL}dd}&0\\0&Y_{\mathrm{GFL}qq}\end{bmatrix}\begin{bmatrix}0&-\omega_{\mathrm{GFM0}}L_{\mathrm{Line}}\\\omega_{\mathrm{GFM0}}L_{\mathrm{Line}}&0\end{bmatrix}\\&=\begin{bmatrix}0&-\omega_{\mathrm{GFM0}}L_{\mathrm{Line}}Y_{\mathrm{GFL}dd}\\\omega_{\mathrm{GFM0}}L_{\mathrm{Line}}Y_{\mathrm{GFL}qq}&0\end{bmatrix}.\end{aligned}\tag{9}$$

Still, $\mathbf{Z}_{\mathrm{GFM}}$ is approximated as $\mathbf{Z}_{\mathrm{Line}}$.

Besides, by neglecting the voltage drop on the filter inductance and approximating $\mathbf{Tran}(\delta_0)$ to an identity matrix, $-\mathbf{T}_{\omega\mathrm{GFL}}\mathbf{T}_{\omega\mathrm{GFM}}$ can be obtained as

$$-\mathbf{T}_{\omega\mathrm{GFL}}\mathbf{T}_{\omega\mathrm{GFM}}\approx-G_p\begin{bmatrix}V_{d0}T_{\omega\mathrm{GFL}d}&0\\V_{d0}T_{\omega\mathrm{GFL}q}&0\end{bmatrix}\tag{10}$$

where $T_{\omega\mathrm{GFL}\,d}$ and $T_{\omega\mathrm{GFL}\,q}$ represent the d-axis and q-axis elements of $\mathbf{T}_{\omega\mathrm{GFL}}$, respectively. According to Fig. 4, $\mathbf{T}_{\omega\mathrm{GFL}}$ will be shaped by PLL-related matrices $\mathbf{G}_{fi\text{-PLL}}$, $\mathbf{G}_{fv\text{-PLL}}$, and $\mathbf{G}_{fd\text{-PLL}}$. Moreover, the elements on the d-axis of the above matrices are related to voltage/current on the q-axis, larger than the elements on the q-axis, which are determined by voltage/current on the d-axis. Take $\mathbf{G}_{fi\text{-PLL}}$ in (5) as an example: the d-axis element is related to I_{q0} while the q-axis element is related to I_{d0}. Hence, $T_{\omega\mathrm{GFL}\,d}$ will have a smaller amplitude than $T_{\omega\mathrm{GFL}\,q}$, and (10) can be simplified as

$$-\mathbf{T}_{\omega\mathrm{GFL}}\mathbf{T}_{\omega\mathrm{GFM}}\approx-G_p\begin{bmatrix}0&0\\V_{d0}T_{\omega\mathrm{GFL}q}&0\end{bmatrix}.\tag{11}$$

Summarizing (8), (9), and (11), we have

$$\mathbf{L}\approx\begin{bmatrix}0&-\omega_{\mathrm{GFM0}}L_{\mathrm{Line}}Y_{\mathrm{GFL}dd}\\\omega_{\mathrm{GFM0}}L_{\mathrm{Line}}Y_{\mathrm{GFL}qq}-G_pV_{d0}T_{\omega\mathrm{GFL}q}&0\end{bmatrix}.\tag{12}$$

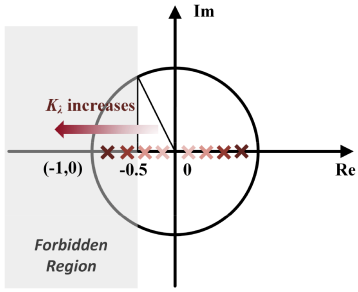

Fig. 7. Forbidden region by opposing argument (OA) criteria.

Therefore, the eigenvalue $\lambda_{1,2}$ of $\mathbf{L}$ can be calculated as

$$\lambda_{1,2}{}^2=\underbrace{\overbrace{-\omega_{\mathrm{GFM0}}^2L_{\mathrm{eq}}^2Y_{\mathrm{GFL}dd}Y_{\mathrm{GFL}qq}}^{\text{First term}}+\overbrace{\omega_{\mathrm{GFM0}}L_{\mathrm{eq}}Y_{\mathrm{GFL}dd}G_pV_{d0}T_{\omega\mathrm{GFL}q}}^{\text{Second term}}}_{K_\lambda}.\tag{13}$$

A real value K_λ is approximated in (13), whose sign can be used for stability assessment. At low frequencies, $Y_{\mathrm{GFL}\,dd}$ and $Y_{\mathrm{GFL}\,qq}$ can be regarded as positive conductance and negative conductance [5]. Moreover, according to the analysis in Section II-C, the current response $T_{\omega\mathrm{GFL}\,q}$ of GFL-VSC under frequency perturbation is also a positive value. Hence, both the first and second terms of K_λ are of positive values, leading to two eigenvalues located on the negative and positive real axes.

Furthermore, a low PLL bandwidth will lead to an enlarged value of $T_{\omega\mathrm{GFL}\,q}$, further increasing the value of K_λ and driving the eigenvalues to more positive or negative values. According to the theory of forbidden region [18], the aforementioned process may lead to the eigenvalues moving deeper into the forbidden region, as shown in Fig. 7, deteriorating system stability.

As some assumptions have been used in the aforementioned analysis to provide concise expressions with physical interpretations, the derived conclusions may be influenced by various operation conditions. The main assumption related to the operation condition is that the GFL-VSC operates under unity power factor, so that the nondiagonal elements of $\mathbf{Y}_{\mathrm{GFL}}$ will have much smaller amplitudes than the diagonal elements, and the d-axis element of $\mathbf{T}_{\omega\mathrm{GFL}}$ will also have smaller amplitudes than its q-axis element. Numerical analysis has shown that the validity of such an assumption will be deteriorated under decreased power factors but will remain mostly solid when the power factor ranges in 0.9–1, serving as an acceptable representative for industry cases.

It should also be noted that the above stability analysis is not aimed to provide a quantitative estimation of the stability boundary, but to provide physical insights on why such kind of instability exists and will happen at low PLL bandwidth. Therefore, the used assumptions serve as a feasible tool for intuitive analysis of system stability.

As a conclusion, two different types of instability related to PLL may be observed for interconnected GFM- and GFL-VSCs.

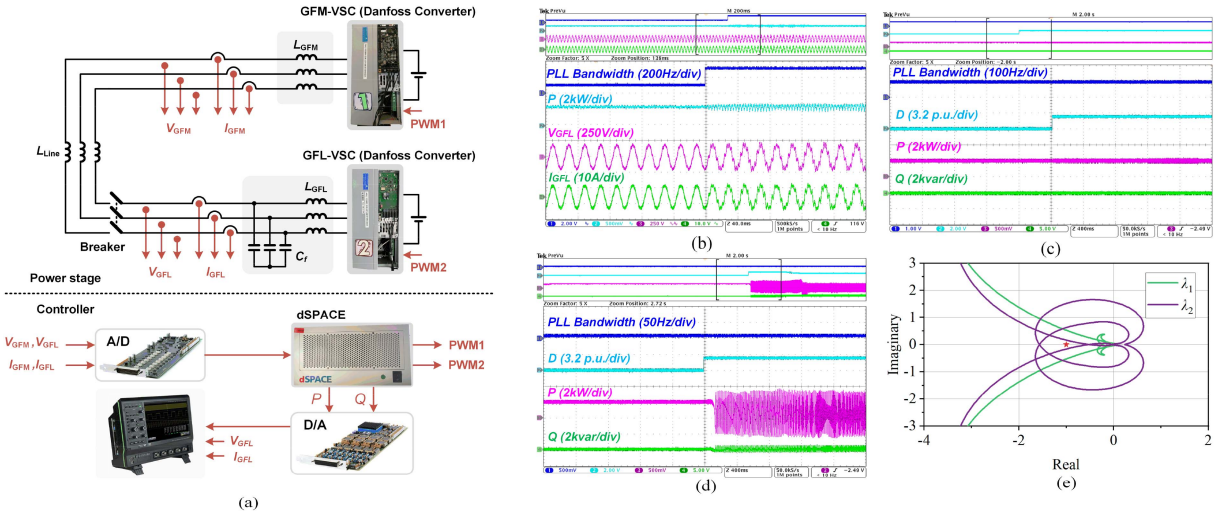

Fig. 8. (a) Experimental setup. (b) System becomes unstable when increasing the PLL bandwidth from 100 to 320 Hz. (c) With PLL bandwidth of 100 Hz, system remains stable when the droop parameter increases. (d) With PLL bandwidth of 10 Hz, system becomes unstable when the droop parameter increases, due to the interaction of synchronization controllers. (e) Eigenloci for the unstable case in (d).

TABLE I
PARAMETERS FOR THE EXPERIMENTAL VALIDATIONS

Description	Value
Rated power	2 kW (1 p. u.)
Voltage (RMS)	110 V (50 Hz) (1 p. u.)
GFL-VSC filter inductance L_{GFL}	3 mH (0.07 p. u.)
GFL-VSC current controller (P/I)	2.8 / 70 p.u.
GFL-VSC PLL (Bandwidth = 100 Hz) (P/I)	1.5 / 352.6 p.u.
GFL-VSC power controller (P/I)	0.05 / 10 p.u.
GFM-VSC filter inductor L_{GFM}	3 mH (0.07 p. u.)
GFM-VSC PSC controller (G_p/ω_f)	0.0032 / 1 p.u.
Line inductance L_{Line}	5 mH (0.12 p. u.)

When PLL bandwidth is high, the instability may happen due to the interaction of terminal impedances. When PLL bandwidth is low, the instability may occur due to the interaction of synchronization controllers, which has rarely been reported in the existing research. Moreover, this newly observed instability with low PLL bandwidth will not be influenced by the filter types of the converters. This is because the studied instability happens at low frequency, making the influence of the capacitor components in the filters negligible. Therefore, the analysis and conclusion of this letter can be generalized to converter systems with different types of filters.

IV. EXPERIMENTAL VALIDATIONS

Experiments have been conducted for validation purposes, with configurations in Fig. 8(a) and parameters in Table I.

System instability with high PLL bandwidth is first tested in Fig. 8(b), where the PLL bandwidth increases from 100 to 320 Hz. Furthermore, the instability at low PLL bandwidth can be observed in Fig. 8(d), with a stable operation case presented in Fig. 8(c) as a comparison. It is shown that when G_p increases to a large value (2.4 p.u. in the experiments), the system remains stable at higher PLL bandwidth [100 Hz in Fig. 8(c)] and

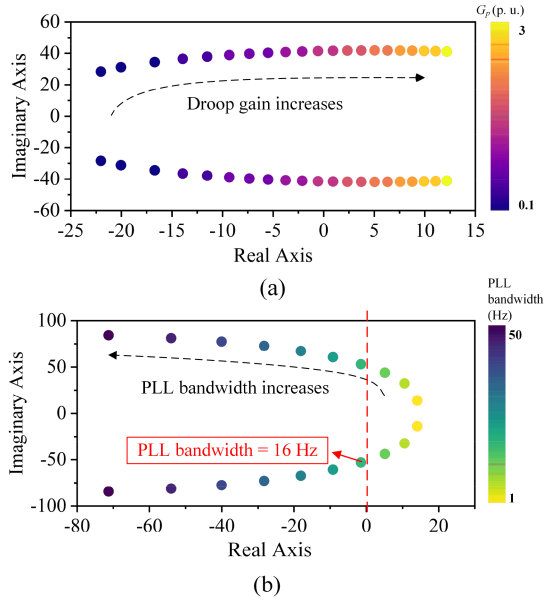

Fig. 9. Pole trajectory under different PLL bandwidth and droop gain. (a) PLL bandwidth is set at 10 Hz, while the droop gain increases. (b) Droop gain is set as 2.4 p.u., while the PLL bandwidth varies.

becomes unstable at lower PLL bandwidth [10 Hz in Fig. 8(d)]. The eigenloci of $\mathbf{L}$ in Fig. 8(d) are also presented in Fig. 8(e). It is shown that $(-1 + j0)$ point is encircled, supporting the effectiveness of the modeling and stability analysis.

To further reveal how the PLL bandwidth and droop gain G_p affect system stability, the trajectory for the pair of poles related to this low-frequency instability is plotted in Fig. 9. The poles are calculated by solving the roots of the determinant for $\mathbf{I} + \mathbf{L}$. $\mathbf{L}$ is calculated based on (8) using the small-signal models in Section II.

Fig. 9 shows that the damping of the system decreases when the droop gain increases and PLL adopts a lower bandwidth,

as the poles will gradually move to the right-half-plane. As a conclusion, the interaction of PLL and PSC may deteriorate system stability and push the system to the stability boundary in practices, which should be holistically treated by the system designers.

Besides, the calculated pole trajectory can also be used to determine the lower limit of the PLL bandwidth for system stable operation. It is shown in Fig. 9(b) that a typical value for the lower limit of the PLL bandwidth can be set as 16 Hz in the studied case. The upper limit of the PLL bandwidth can also be obtained by pole trajectory analysis similarly [4], which will not be detailed for simplicity.

As the physical insight of this newly observed instability phenomenon lies in that the GFL-VSC may lose track of system frequency dynamics when using low PLL bandwidth, one solution to stabilize the system could be applying the mode-adaptive power-angle control in the GFM-VSC. The droop gain of the PSC in GFM-VSC can be decreased to a smaller value in a protection mode when system instability is detected, to prevent the GFL-VSC from losing track of the phase angle and to maintain system stable operation.

V. Conclusion

This letter has studied the influence of PLL bandwidth on the stability of interconnected GFM- and GFL-VSCs, by small-signal stability analysis. Two different types of instability have been identified and analyzed, which are caused by: 1) interaction between terminal impedance when PLL bandwidth is high with GFL-VSC; and 2) interaction between synchronization controllers when PLL bandwidth is low with GFL-VSC. The latter one has rarely been reported in the existing research. Experiments validate the effectiveness of the theoretical analysis.

References

[1] B. Wen, R. Burgos, D. Boroyevich, P. Mattavelli, and Z. Shen, "AC stability analysis and *dq* frame impedance specifications in power-electronics-based distributed power systems," *IEEE J. Emerg. Sel. Topics Power Electron.*, vol. 5, no. 4, pp. 1455–1465, Dec. 2017.

[2] S. Wang, Z. Liu, J. Liu, D. Boroyevich, and R. Burgos, "Small-signal modeling and stability prediction of parallel droop-controlled inverters based on terminal characteristics of individual inverters," *IEEE Trans. Power Electron.*, vol. 35, no. 1, pp. 1045–1063, Jan. 2020.

[3] E. A. S. Ducoin, Y. Gu, B. Chaudhuri, and T. C. Green, "Analytical design of contributions of grid-forming & grid-following inverters to frequency stability," *IEEE Trans. Power Syst.*, early access, Jan. 9, 2024, doi: 10.1109/TPWRS.2024.3351530.

[4] D. P. Morán-Río, J. Roldán-Pérez, M. Prodanović, and A. García-Cerrada, "Influence of the phase-locked loop on the design of microgrids formed by diesel generators and grid-forming converters," *IEEE Trans. Power Electron.*, vol. 37, no. 5, pp. 5122–5137, May 2022.

[5] B. Wen, D. Boroyevich, R. Burgos, P. Mattavelli, and Z. Shen, "Analysis of D-Q small-signal impedance of grid-tied inverters," *IEEE Trans. Power Electron.*, vol. 31, no. 1, pp. 675–687, Jan. 2016.

[6] D. Dong, B. Wen, D. Boroyevich, P. Mattavelli, and Y. Xue, "Analysis of phase-locked loop low-frequency stability in three-phase grid-connected power converters considering impedance interactions," *IEEE Trans. Ind. Electron.*, vol. 62, no. 1, pp. 310–321, Jan. 2015.

[7] C. Tu, J. Gao, F. Xiao, Q. Guo, and F. Jiang, "Stability analysis of the grid-connected inverter considering the asymmetric positive-feedback loops introduced by the PLL in weak grids," *IEEE Trans. Ind. Electron.*, vol. 69, no. 6, pp. 5793–5802, Jun. 2022.

[8] F. Chan, L. Zhao, L. Harnefors, X. Wang, J. Kukkola, and M. Routimo, "Enhance Q-axis voltage-integral damping control for fast PLL-synchronized inverters in weak grids," *IEEE Trans. Power Electron.*, vol. 39, no. 1, pp. 424–435, Jan. 2024.

[9] M. Naderi, Y. Khayat, Q. Shafiee, T. Dragičević, H. Bevrani, and F. Blaabjerg, "Interconnected autonomous ac microgrids via back-to-back converters—Part I: Small-signal modeling," *IEEE Trans. Power Electron.*, vol. 35, no. 5, pp. 4728–4740, May 2020.

[10] J. Fang, H. Deng, N. Tashakor, F. Blaabjerg, and S. M. Goetz, "State-space modeling and control of grid-tied power converters with capacitive/battery energy storage and grid-supportive services," *IEEE J. Emerg. Sel. Topics Power Electron.*, vol. 11, no. 1, pp. 234–250, Feb. 2023.

[11] Y. Liao, X. Wang, and X. Wang, "Frequency-domain participation analysis for electronic power systems," *IEEE Trans. Power Electron.*, vol. 37, no. 3, pp. 2531–2537, Mar. 2022.

[12] HVDC Wise, "Deliverable 4.1: Identification of key technologies, potential benefits and restrictions," 2023. [Online]. Available: https://hvdc-wise.eu/resources/

[13] D. Groß, E. Sánchez-Sánchez, E. Prieto-Araujo, and O. Gomis-Bellmunt, "Dual-port grid-forming control of MMCs and its applications to grids of grids," *IEEE Trans. Power Del.*, vol. 37, no. 6, pp. 4721–4735, Dec. 2022.

[14] "Deliverable 2.4: Requirement recommendations to adapt and extend existing grid codes," 2019. [Online]. Available: https://www.promotion-offshore.net/results/deliverables/

[15] Z. Liu, J. Liu, and D. Boroyevich, "Small-signal terminal characteristics modeling of three-phase boost rectifier with variable fundamental frequency," in *Proc. IEEE Appl. Power Electron. Conf. Expo.*, 2016, pp. 739–745.

[16] S. Skogestad and I. Postlethwaite, *Multivariable Feedback Control: Analysis and Design*. Hoboken, NJ, USA: Wiley, 2007.

[17] F. Zhao et al., "Control interaction modeling and analysis of grid-forming battery energy storage system for offshore wind power plant," *IEEE Trans. Power. Syst.*, vol. 37, no. 1, pp. 497–507, Jan. 2022.

[18] A. Riccobono and E. Santi, "Comprehensive review of stability criteria for DC power distribution systems," *IEEE Trans. Ind. Appl.*, vol. 50, no. 5, pp. 3525–3535, Sep./Oct. 2014.